Measurement of the composite muon lifetime, mass and determination of the Fermi coupling constant

Kailas Amin,[*] Vassilios Kaxiras,[†] and Austin W. Li[‡]

Department of Physics, Harvard University, Cambridge, Massachusetts 02138, USA

(Dated: December 7, 2022)

Muons are a key component of the standard model, playing a central role in understanding electroweak theory. Diverse applications across science (special relativity; industrial sensing; archaeological discovery), make understanding muon properties extremely valuable. We provide high fidelity measurements of the muon lifetime and mass, and use them to compute the Fermi coupling constant G_F. Through use of three p-terphenyl doped plastic scintillators, each attached to highly charged photomultiplier tubes, we identify muons which come to rest in the detector and magnify their decay-electron signals to levels which can be accurately measured. We determine a composite (positive and negative muon) lifetime of $\tau_\mu = 2.037 \pm 0.013$ μs. Additionally, we compute the rest mass of a muon to be $m_\mu = 106 \pm 18$ MeV/c^2. We then estimate $G_F = 1.20 \pm 0.45 \times 10^{-5}$ GeV^{-2}. Our results are similar to those in the literature and demonstrate additional confirmation for the muon predictions of the standard model.

I. INTRODUCTION

Muons are one of the fundamental subatomic particles described by the standard model [1]. Muons were discovered by Neddermeyer and Anderson in 1937 [2]. The collision of the high-energy proton cosmic rays and atomic nuclei in the atmosphere produce pions and mesons which in turn decay into muons and neutrinos [3]. Williams and Roberts conducted the first observation of muon decay in 1940, shortly after the discovery of the muon[4].

The detection and understanding of muons is important in a diverse set of fields [5–7]. Beyond their central role in the standard model and electroweak theory, the measurement of muons at sea level has also provided precise measurements of time dilation [8, 9]. The study of muons even has applications in archaeology and industrial sensing where they are used to scan large, dense objects such as nuclear reactors and the Pyramids of Giza [10, 11].

We utilize three doped-plastic scintillators in combination with both analog and digital control equipment to determine accurate measurements of two key properties of muons: their mass and lifetime.

II. BACKGROUND

The vast majority of muons are produced as a result of pion decay following Eq. 1.

$$\pi^+ \to \mu^+ + \overline{\nu}_\mu, \qquad \pi^- \to \mu^- + \nu_\mu, \qquad (1)$$

where π, μ, and ν denote pions, muons, and neutinos, respectively [1]. The superscript denotes charge parity, and

---

[*] kailasamin@college.harvard.edu

[†] vkaxiras@college.harvard.edu

[‡] awli@college.harvard.edu

the bar denotes an antiparticle. Moreover, we note that neutrinos come in three flavors, ν_e, ν_μ, ν_τ which denote electron, muon, and tau neutrinos, respectively.

The muons resulting from these decays travel at near light speed and thus, as a result of time dilation, the vast majority reach sea level despite having a rest lifetime on the order of microseconds [8, 9]. Under our experimental conditions (near sea level, moderate latitude) the expected muon flux is on the order of 10^{-2}cm^{-2} sr s^{-1} [12]. A small fraction of muons come to rest in our scintillation apparatus and decay as shown in Eq. 2. By examining the electron that results from this decay, we can understand muon properties.

$$\mu^+ \to e^+ + \overline{\nu}_\mu + \nu_e, \qquad \mu^- \to e^- + \nu_\mu + \overline{\nu}_e. \qquad (2)$$

During the course of muon collection, both positive and negative muons contact the apparatus. The relative frequency of positive and negative muons is the subject of active research, and indeed they have a close relationship to the frequency of positive and negative neutrinos, whose observed frequencies do not align with the predictions of the standard model [13]. The two species interact differently with the scintillation apparatus. Negatively charged muons may be trapped by atoms of the collection medium forming a neutron from a proton in an atomic nucleus as shown in Eq. 3:

$$\mu^- + p^+ \to n + \nu_\mu \qquad (3)$$

where p is the proton and n is the neutron [1, 13]. Positively charged muons are weakly interactive and can sometimes be completely missed by the apparatus.

The two species also have slightly different lifetimes [13]. The literature suggests this distinction is no more than 0.005 μs[1, 9, 13]. This is dominated by experimental error in our apparatus. In this experiment, we focus on composite values for both muon energy and lifetime.

III. EXPERIMENTAL SETUP

A. Scintillation detectors and photomultiplier tubes

We use three plastic scintillation detectors to detect muon events. The detectors are stacked vertically and made of a clear plastic wrapped with a reflective inner layer in combination with a photo-absorbent outer layer to trap muon decay products and prevent interference from ambient light. The plastic blocks are doped with p-terphenyl, a phosphorescent material, so that they emit light pulse when exposed to an ionizing particle. Each detector is coupled to a photomultiplier tube (PMT) made with the same plastic without the phosphorescent material.

The PMTs consist of a series of negatively charged dynodes, electrodes in a vacuum tube that serve as electron multipliers. When a photon of a certain energy strikes the cathode (operated at a large negative voltage), an electron is liberated via the photoelectric effect. The electron is then accelerated towards the dynode and liberates several electrons from each dynode in sequence, generating a powerful cascade. This series of dynodes magnifies the original signal, multiplying its intensity by a factor of 10^6 to 10^8, resulting in an observable magnitude.

B. Nuclear instrumentation modules (NIM)

We use a discriminator (Lecroy 821) to process electrical pulses from the PMTs. In particular, we use discriminators to reject small signals and other electronic noise specified below a specified threshold. The pulse polarity from PMTs is negative; if the amplitude of an input pulse is greater than the threshold, the discriminator returns an output logic pulse. We can also adjust the width of the logic pulses.

We use concidence units (LeCroy 622) to apply logic gates to pairs of NIM outputs from the discriminator. Supported operations include AND, OR, and NOT. A Lecroy 428F linear fan-out unit also supports two linear FANOUT gates built into each NIM package.

We also use a gate generator (LeCroy 222) to configure different gates, including START, STOP, and GATE, which we use in conjunction with the coincidence units to define when muon events should be captured by a digital storage oscilloscope (Tektronix DPO3014).

A START gate indicates when a muon passes through the top scintillator and halts in the middle scintillator; STOP indicates a muon (decay) event in the middle scintillator after a START signal. We define START = T ∧ M ∧ ¬B and STOP = GATE ∧ M where T, M, B correspond to signals from the top, middle, and bottom scintillators, respectively. GATE is an open logic gate with a width of 16 μs, importantly on the order of many muon lifetimes. Moreover, GATE is triggered with a de-

lay of 60 ns after the START signal to prevent double counting. The full instrumental module setup is shown in Fig. 1.

C. Computer control

We use LabVIEW virtual instrumentation to measure muon and electron events and sort them into bins by frequency. We use three software packages written by Joseph Peidle to collect muon mass, muon lifetime, and electron energy calibration data. After binning and basic pre-processing, we conduct our own analysis.

IV. MUON LIFETIME

A. Initial fit

We investigate the muon lifetime by observing its decay at rest. Specifically, we consider only muons that pass through the top scintillator and come to a halt in the middle scintillator in our setup. After the decay event, the resulting positron or electron is detected by the middle scintillator. The distribution of the time difference between the incidence of the muon and the appearance of the decay products over many decay events gives the decay probability as a function of time. Discretizing this distribution into n bins of width Δt, we fit it via least-squares to an exponential of the form:

$$p_m \propto e^{-\Gamma n \Delta t} \tag{4}$$

where p_m is the probability of the muon decaying in a time within bin n, and Γ is a fit parameter. This allows us to extract the half-life as $\tau_\mu = 1/\Gamma$. Collecting 12670 decay events over six days of recording, we obtain the data and fit shown in Fig. 2a.

B. Error analysis and corrections

One source of error is a result of additional muon transits within the lifetime of the initial START reading. This creates a false STOP event artificially reducing the measured lifetime. This adds false decay events uniformly across time which constitute approximately 0.1% of total readings. To correct for these errors, we add a parameter B to the probability fit.

A second source of error is PMT afterpulsing, resulting from random emission within PMT tubes. Secondary PMT electron avalanches which start at a leading plate may magnify to a voltage sufficient to generate a false reading, artificially reducing measured lifetime. Our choice of digital logic apparatus and careful tuning of detection thresholds eliminates all but the largest cascades. In addition, we choose to discard data below a certain cutoff decay time $t_{\min}$. Since the probability of
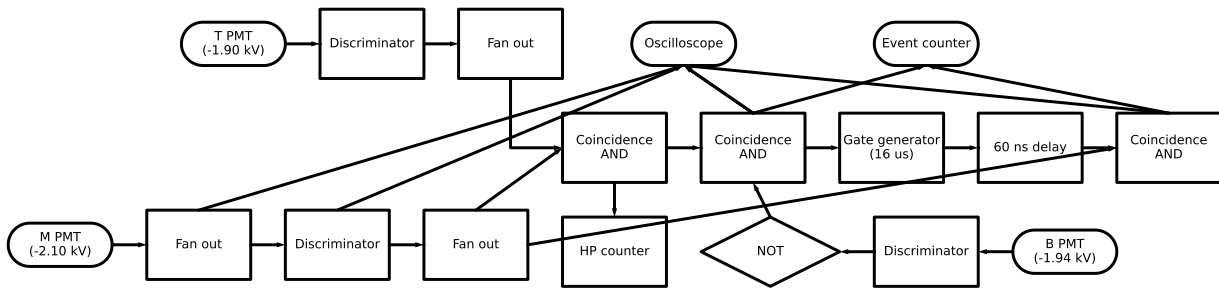
FIG. 1: Schematic of connections between logic and coincidence units for muon lifetime and mass measurements. T, M, and B denote signals from the top, middle, and bottom scintillators, respectively.

a PMT afterpulse decreases rapidly with increasing time from the original event, we expect τ_μ to converge to its true value for increasing $t_{\min}$.

A third source of error is the distinction between negative and positive muons. Since negative muons can interact with atoms, forming bound states or being completely captured by nuclei, high-energy atom-muon interactions can produce false STOP events, skewing the lifetime measurements to lower values. We cannot account for such complex events, besides expecting some systematic error in our results.

Accounting for the first two sources of error and choosing a value of $t_{\min}$ in the plateau region we measure a revised lifetime of $\tau_\mu = 2.037 \pm 0.013$ μs with $R^2 = 0.0227$, shown in Fig. 2b.

V. MUON MASS

A. Calibration

We measure the mass of stopped muons by characterizing the distribution of their electron decay products. The three-body decay process of Eq. 2 imparts maximal momentum in the electron when both neutrinos move anti-parallel to the electron. In this case, neglecting the neutrino mass (because the muon is roughly 200 times heavier), the energy of the electron is proportional to its momentum and thus equal to half the muon rest mass. Observing the maximum energy of an electron produced by a muon decaying from rest will give an estimate of the muon mass.

We calibrate the energy of decay products in our apparatus by comparing the energies deposited by muons passing through the middle scintillator with an expected muon ionizing energy distribution derived from the literature. We were careful to choose the dynode voltages such that we operate in the linear (between pulse current

and ionizing energy) regime of the PMT.

A widely accepted expression for the flux of muons of energy E at sea level is the Gaisser model [14]. Neglecting variations in the incident polar angle gives a muon flux $\Phi(E) \propto E^{-2.7}$. Using the Bethe-Bloch formula [15] for the ionizing energy per unit distance dE/dx as a function of incident muon energy E, we can obtain the flux $\Phi^{(n)}$ of muons with ionizing energies in the range $s \times dE/dx \in [E_I^{(n)}, E_I^{(n)} + \Delta E_I)$, where $\{E_I^{(n)}\}$ form an evenly-spaced discretization of the ionizing energy range we are interested in. We let $s = 2.5$ cm, which corresponds to the width of each scintillator. $\Phi^{(n)}$ is given by

$$\Phi^{(n)} \propto \int_{-\infty}^{\infty} S\left[\frac{s \times \frac{dE}{dx}\big|_E - E_I^{(n)}}{\Delta E_I}\right] \Phi(E)\, dE \qquad (5)$$

where we define

$$S(x) \equiv \begin{cases} 1, & 0 \le x < 1 \\ 0, & \text{otherwise} \end{cases}. \qquad (6)$$

Choosing a width of $E_I^{(n+1)} - E_I^{(n)} = 0.25$ MeV, we extract the theoretically predicted most probable ionizing energy $E_I^{(n_{\max})} = \mathrm{argmax}_n\ \Phi^{(n)}$ in Fig. 3a, and equate it to the most probable observed muon pulse height in Fig. 3b to calibrate the relationship between PMT signal height and ionizing energy. The pulse heights are computed as the peak-to-peak voltages of pulses from the PMT with a 50 Ω load. We focus on muons that pass through all three scintillators, discarding those that stop. This gives a relationship between ionizing energy and PMT signal of 7.25 ± 0.125 MeV/0.062 ± 0.01 V.
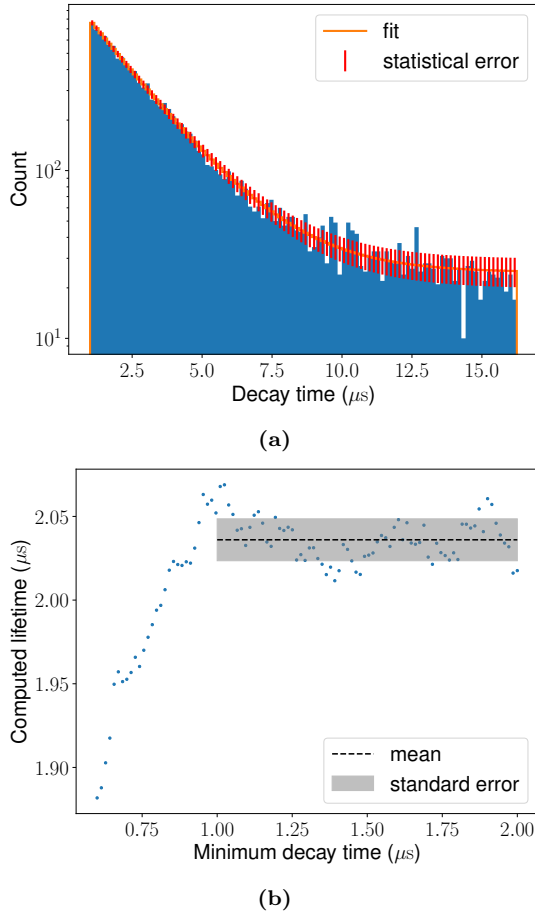
(a)

(b)

FIG. 2: (2a) Histogram of 12670 muon decay events, fitted via least-squares to the function $P(t) = Ae^{-\Gamma t} + B$, with statistics $\chi^2 = 113.2$, $p = 0.1559$. The minimum cutoff for the decay time is 1.1 μs, and the bin size is 0.152 μs. The extracted muon lifetime is $\tau_\mu = 2.033$ μs. (2b) Muon decay lifetime τ_μ as a function of cutoff time $t_{\min}$. The mean and one standard deviation error of the plateau region are labelled by the dashed black line and grey region, respectively. The primary purpose of this analysis is to determine the plateau region. Statistical errors were estimated using a binomial distribution of independent variables for each discretization bin.

B. Deposited energy

We record the energy of electrons produced in the decay of muons at rest in the middle scintillator of our setup. Their distribution displays a Boltzmann tail, which we fit via least-squares. We extract a cutoff maximum electron energy of 0.45 ± 0.01 V. Events above this energy deviate from the standard error boundaries in the fit; this may be due to noise from the PMT or stray high-energy particles, including other muons. Using the maximal electron energy, which we expect to be half the muon mass, we obtain a muon mass value of
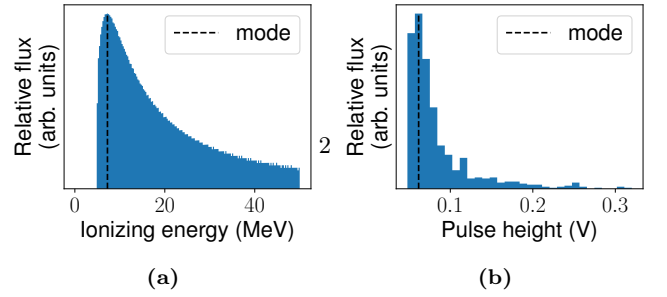

(a)   **(b)**

FIG. 3: (3a) Expected relative flux of muons at polar angle $\theta = 0$ computed using the Bethe-Block and Gaisser models. The mode (most probable sector), used for calibration, is highlighted. (3b) Observed pulse height distribution from the middle scintillator for muons passing through all three scintillators. The mode is highlighted. We are primarily concerned with peak location, thus x-axis errors of magnitude one histogram bin predominate.
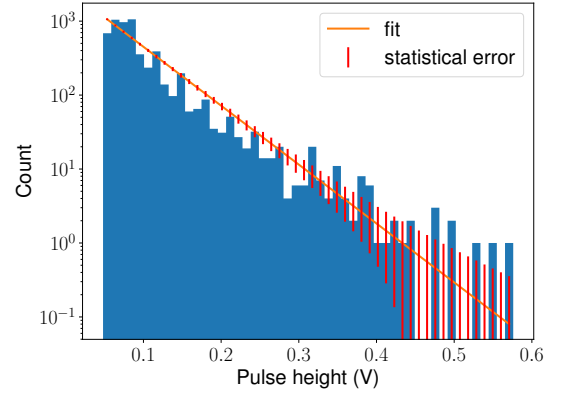

FIG. 4: Histogram of 5719 PMT pulses from electrons produced by muon decay. The pulse height is proportional to the electron energy, by a factor $(9 \pm 1) \times 10^{-3}$ V/MeV. The fit is an exponential of the form Ae^{-h/h_0}, where h is the pulse height and A, h_0 are fit parameters. We are primarily interested in the maximum electron energy before outliers due to stray cosmic rays or other noise, which we determine from the data to be 0.45 ± 0.01 V. Statistical errors were estimated using a binomial distribution of independent variables for each discretization bin.

$m_\mu = 106 \pm 18$ MeV/c^2 where the uncertainty is due to statistical error in quadrature.

C. Error analysis

The large uncertainty present in our mass measurement is largely as a result of low-precision calibration resulting from technical limitations. Our analysis program used relatively coarse binning and as a result, the energy level corresponding to the minimum ionizing muon

is difficult to determine exactly. This large uncertainty propagates throughout the entire calculation, resulting in wide confidence intervals and dominating all other errors.

VI.   DISCUSSION AND COUPLING CONSTANT

Our measured lifetimes and masses are similar to those computed in the literature. Experimental literature suggests a composite lifetime of $\tau_\mu = 2.1975 \pm 0.004$ μs [13] and theoretical predictions of the standard model suggest a lifetime of $\tau_\mu = 2.197$ μs [5, 16]. Experimental investigations of the muon mass observe values of $m_\mu = 105.65932 \pm 0.00029$ MeV/c^2 [17]. We discuss several sources of both systematic and statistical error in previous sections, and examine how they could help explain the discrepancy between our result.

We also compute the Fermi constant using

$$\tau_\mu = \frac{192\pi^3\hbar^7}{G_F^2 m_\mu^5 c^4}, \tag{7}$$

where G_F is the Fermi constant, τ_μ is the muon half-life, and m_μ is the muon mass [18]. We compute a Fermi constant of $G_F = 1.20 \pm 0.45 \times 10^{-5}$ GeV^{-2}, which is similar to the widely accepted value of $1.1663716 \pm 0.0000005 \times 10^{-5}$ GeV^{-2} [16]. The wide confidence intervals in our mass measurement propagate through to this calculation, but strong agreement of the central value is encouraging. Taking into account all of these factors, our measurements support existing theory and help confirm the muon predictions of the standard model.

VII.   FUTURE WORK

More work is needed to develop a clearer understanding of the distinction between positive and negative muons. A more sophisticated detection apparatus and mathematical techniques are needed to differentiate between their individual behaviors. Relative measurements of positive and negative neutrinos are a significant deviation between the standard model and experimental reality. Thus, more clearly understanding their source, positive and negative muons, should be of principal interest to the particle physics community.

VIII.   ACKNOWLEDGEMENTS

We would like to thank Professor Isaac Silvera and Professor Amir Yacoby for their wonderful theoretical and experimental guidance on the project. In addition, Joseph Peidle, Jieping Fang provided invaluable assistance on the experimental setup. Professor Melissa Franklin provided insightful direction for literature review and help with understanding theoretical components of particle physics.

Amin, Kaxiras, and Li collected data, wrote all components of the paper, developed theoretical models, conducted error analysis, and interpreted results. Experimental design/optimization was primarily done by Amin, with the help of Kaxiras and Li. Data analysis code was primarily written by Kaxiras, with the help of Amin and Li. Literature review, calculation of the physical coupling constant, and its comparison to literature was primarily done by Li, with the help of Amin and Kaxiras.

[1] S. F. Novaes, Standard model: An introduction, arXiv preprint hep-ph/0001283 (2000).

[2] S. H. Neddermeyer and C. D. Anderson, Note on the nature of cosmic-ray particles, Physical Review **51**, 884 (1937).

[3] G. Bazilevskaya, I. Usoskin, E. Flückiger, R. Harrison, L. Desorgher, R. Bütikofer, M. Krainev, V. Makhmutov, Y. I. Stozhkov, A. Svirzhevskaya, *et al.*, Cosmic ray induced ion production in the atmosphere, Space Science Reviews **137**, 149 (2008).

[4] E. J. Williams and G. Roberts, Evidence for transformation of mesotrons into electrons, Nature **145**, 151 (1940).

[5] F. Jegerlehner and A. Nyffeler, The muon g- 2, Physics Reports **477**, 1 (2009).

[6] M. Endo, K. Hamaguchi, S. Iwamoto, and T. Kitahara, Supersymmetric interpretation of the muon g–2 anomaly, Journal of High Energy Physics **2021**, 1 (2021).

[7] G. Arcadi, L. Calibbi, M. Fedele, and F. Mescia, Muon g- 2 and b anomalies from dark matter, Physical review letters **127**, 061802 (2021).

[8] S. Tsuji, T. Katayama, K. Okei, T. Wada, I. Yamamoto, and Y. Yamashita, Measurements of muons at sea level, Journal of Physics G: Nuclear and Particle Physics **24**, 1805 (1998).

[9] N. Easwar and D. A. MacIntire, Study of the effect of relativistic time dilation on cosmic ray muon flux—an undergraduate modern physics experiment, American Journal of Physics **59**, 589 (1991).

[10] E. Köhler, R. Bergmann, H. Daniel, P. Ehrhart, and F. Hartmann, Application of muonic x-ray techniques to the elemental analysis of archeological objects, Nuclear Instruments and Methods in Physics Research **187**, 563 (1981).

[11] L. Oláh, G. Barnaföldi, G. Hamar, H. Melegh, G. Surányi, and D. Varga, Ccc-based muon telescope for examination of natural caves, Geoscientific Instrumentation, Methods and Data Systems **1**, 229 (2012).

[12] E. V. Bugaev, A. Misaki, V. A. Naumov, T. Sinegovskaya, S. Sinegovsky, and N. Takahashi, Atmospheric muon flux at sea level, underground, and underwater, Physical Review D **58**, 054001 (1998).

[13] S. Meyer, E. Anderson, E. Bleser, I. Lederman, J. Rosen, J. Rothberg, and I.-T. Wang, Precision lifetime measurements on positive and negative muons, Physical Review **132**, 2693 (1963).

[14] N. Su, Y. Liu, L. Wang, B. Wu, and J. Cheng, A comparison of muon flux models at sea level for muon imaging and low background experiments, Frontiers in Energy Research **9**, 750159 (2021).

[15] D. C. Foudas, Particle physics, 4th year Physics at Imperial.

[16] D. Chitwood, T. Banks, M. Barnes, S. Battu, R. Carey, S. Cheekatmalla, S. Clayton, J. Crnkovic, K. Crowe, P. Debevec, *et al.*, Improved measurement of the positive-muon lifetime and determination of the fermi constant, Physical review letters **99**, 032001 (2007).

[17] R. Abela, M. Daum, G. Eaton, R. Frosch, B. Jost, P.-R. Kettle, and E. Steiner, Precision measurement of the muon momentum in pion decay at rest, Physics Letters B **146**, 431 (1984).

[18] T. van Ritbergen and R. G. Stuart, On the precise determination of the fermi coupling constant from the muon lifetime, Nuclear Physics B **564**, 343 (2000).